

**Influence of the Pulse Duration in the Anthropomorphic
Test Device (ATD) Lower-Leg Loading Mechanics**

by Masayuki Sakamoto

ARL-SR-0331

August 2015

NOTICES

Disclaimers

The findings in this report are not to be construed as an official Department of the Army position unless so designated by other authorized documents.

Citation of manufacturer's or trade names does not constitute an official endorsement or approval of the use thereof.

Destroy this report when it is no longer needed. Do not return it to the originator.

Army Research Laboratory

Adelphi, MD 20783-1138

ARL-SR-0331

August 2015

Influence of the Pulse Duration in the Anthropomorphic Test Device (ATD) Lower-Leg Loading Mechanics

Masayuki Sakamoto
Japanese ESEP Research Engineer
at Weapons and Materials Research Directorate, ARL

REPORT DOCUMENTATION PAGE			<i>Form Approved</i> OMB No. 0704-0188	
<p>Public reporting burden for this collection of information is estimated to average 1 hour per response, including the time for reviewing instructions, searching existing data sources, gathering and maintaining the data needed, and completing and reviewing the collection information. Send comments regarding this burden estimate or any other aspect of this collection of information, including suggestions for reducing the burden, to Department of Defense, Washington Headquarters Services, Directorate for Information Operations and Reports (0704-0188), 1215 Jefferson Davis Highway, Suite 1204, Arlington, VA 22202-4302. Respondents should be aware that notwithstanding any other provision of law, no person shall be subject to any penalty for failing to comply with a collection of information if it does not display a currently valid OMB control number.</p> <p>PLEASE DO NOT RETURN YOUR FORM TO THE ABOVE ADDRESS.</p>				
1. REPORT DATE (DD-MM-YYYY) August 2015		2. REPORT TYPE ESEP activity		3. DATES COVERED (From - To) 04/2013–09/2014
4. TITLE AND SUBTITLE Influence of the Pulse Duration in the Anthropomorphic Test Device (ATD) Lower-Leg Loading Mechanics			5a. CONTRACT NUMBER	
			5b. GRANT NUMBER	
			5c. PROGRAM ELEMENT NUMBER	
6. AUTHOR(S) Masayuki Sakamoto (Japanese Engineer Scientist Exchange Program Research Engineer)			5d. PROJECT NUMBER ESEP	
			5e. TASK NUMBER	
			5f. WORK UNIT NUMBER	
7. PERFORMING ORGANIZATION NAME(S) AND ADDRESS(ES) US Army Research Laboratory ATTN: RDRL-WMP-F 2800 Powder Mill Road Adelphi, MD 20783-1138			8. PERFORMING ORGANIZATION REPORT NUMBER ARL-SR-0331	
9. SPONSORING/MONITORING AGENCY NAME(S) AND ADDRESS(ES) Survivability and Firepower Analysis Section, Ballistic Research Division, Ground Systems Research Center ATTN: Masayuki Sakamoto 2-9-54, Fuchinobe, Chuo-ku, Sagamihara-shi, Kanagawa-ken 252-0206, JAPAN			10. SPONSOR/MONITOR'S ACRONYM(S)	
			11. SPONSOR/MONITOR'S REPORT NUMBER(S)	
12. DISTRIBUTION/AVAILABILITY STATEMENT Approved for public release; distribution unlimited.				
13. SUPPLEMENTARY NOTES Engineer Scientist Exchange Program between US and Japan Because one of the authors of this report is an employee of the Japanese Ministry of Defense (JMOD), this report cannot be published without approval by the appropriate Japanese organization. At the completion of the formal review process, and before publication, please forward this report to the Technical Research and Development Institute (TRDI), JMOD for approval to publish this report (JMOD/TRDI POC: Mr. Masayuki Sakamoto, Survivability and Firepower Analysis Section, Ballistic Research Division, Ground Systems Research Center [E-mail: masayuki@cs.trdi.mod.go.jp , Phone:+81-42-752-2941, Address:2-9-54, Fuchinobe, Chuo-ku, Sagamihara-shi, Kanagawa-ken 252-0206, JAPAN]). Retain a copy of the approval with the Form-1 record.				
14. ABSTRACT This report was written by the author under the Engineer Scientist Exchange Program in the US Army Research Laboratory (ARL) from April 2013 to September 2014. To understand the loading mechanics of the anthropomorphic test device's (ATD's) lower leg in the presence of the blast-mitigating floor mat, the Finite Element Analysis (FEA) was conducted in various loading conditions. Through the FEA's results, the pulse-duration dependency was indicated in the ATD lower-tibia peak load, and the dependency was confirmed though the loading experiment. The ATD lower-leg loading mechanics are discussed with regard to pulse duration.				
15. SUBJECT TERMS ESEP, blast-mitigating floor mat, CSBES, LS-DYNA				
16. SECURITY CLASSIFICATION OF:			17. LIMITATION OF ABSTRACT UU	18. NUMBER OF PAGES 38
A. Report Unclassified	b. ABSTRACT Unclassified	c. THIS PAGE Unclassified		
			19b. TELEPHONE NUMBER (Include area code) (301) 394-5738	

Contents

List of Figures	iv
List of Tables	v
Acknowledgments	vi
1. Introduction	1
2. Analysis and Experiment Methods	1
2.1 Finite Element Model	1
2.2 Loading Conditions in the FEA.....	4
2.3 Lower-Leg Loading Test	6
3. Results and Discussion	9
3.1 FEA Results	9
3.2 Experimental Results.....	19
3.3 ATD Lower-Leg Loading Mechanics	23
4. Conclusions	26
5. References	28
6. List of Symbols, Abbreviations, and Acronyms	29
Distribution List	30

List of Figures

Fig. 1	FE model for the ATD lower-leg loading.....	2
Fig. 2	Definition of the lower-tibia load Fz in the ATD lower-leg FE model	3
Fig. 3	Definition of the toe part and heel part on the boot sole.....	3
Fig. 4	Schematic of boundary conditions in the FEA.....	5
Fig. 5	Velocity histories on the floor plate in FEAs for 3.0-m/s loading	5
Fig. 6	Velocity histories on the floor plate in FEAs for 6.5-m/s loading	6
Fig. 7	Velocity histories on the floor plate in FEAs for 10-m/s loading	6
Fig. 8	Test setup for the lower leg loading test with the whole-body ATD and floor mat.....	7
Fig. 9	Sheets of the butyl rubber as the floor mat on the CSBES floor plate.....	7
Fig. 10	Arrangements of sensors in the test setup.....	8
Fig. 11	Representative load histories of the ATD lower tibia in the FEA, X065_08 ($\Delta V = 6.5$ m/s, $\Delta T = 8$ msec)	9
Fig. 12	Representative ATD lower-leg motion in the FEA, X065_08 ($\Delta V = 6.5$ m/s, $\Delta T = 8$ msec)	11
Fig. 13	Pressure distribution under the boot sole in the FEA result, X065_02 ($\Delta V = 6.5$ m/s, $\Delta T = 2$ msec).....	11
Fig. 14	Pressure distribution under the boot sole in the FEA result, X065_06 ($\Delta V = 6.5$ m/s, $\Delta T = 6$ msec).....	12
Fig. 15	Pressure distribution under the boot sole in the FEA result, X065_10 ($\Delta V = 6.5$ m/s, $\Delta T = 10$ msec).....	12
Fig. 16	Example of load histories of the ATD lower leg in the FEA, X065_02 ($\Delta V = 6.5$ m/s, $\Delta T = 2$ msec).....	13
Fig. 17	Example of load histories of the ATD lower leg in the FEA, X065_06 ($\Delta V = 6.5$ m/s, $\Delta T = 6$ msec).....	13
Fig. 18	Example of load histories of the ATD lower leg in the FEA, X065_10 ($\Delta V = 6.5$ m/s, $\Delta T = 10$ msec).....	14
Fig. 19	Example of the relation between the peak load and pulse duration on various interfaces in the ATD lower leg, X065 series ($\Delta V = 6.5$ m/s).....	14
Fig. 20	Example of the relation between the applied impulse and pulse duration on various interfaces in the ATD lower leg, X065 series ($\Delta V = 6.5$ m/s).....	15
Fig. 21	Relation between the peak load and pulse duration in the ATD lower-tibia axial force Fz from FEA results.....	16
Fig. 22	Relation between the applied impulse and pulse duration in the ATD lower-tibia axial force Fz from FEA results	16

Fig. 23	Interaction among the ATD foot, boot, and floor mat, X065_02 ($\Delta V = 6.5$ m/s, $\Delta T = 2$ msec).....	17
Fig. 24	Interaction among the ATD foot, boot, and floor mat, X065_06 ($\Delta V = 6.5$ m/s, $\Delta T = 6$ msec).....	17
Fig. 25	Interaction among the ATD foot, boot, and floor mat, X065_10 ($\Delta V = 6.5$ m/s, $\Delta T = 10$ msec).....	17
Fig. 26	Rotation-angle histories of the boot sole against the horizontal line in the FEA, X065 series ($\Delta V = 6.5$ m/s)	18
Fig. 27	Representative load histories of the ATD lower tibia in the experiment, X065_06_03 Right Leg ($\Delta V = 6.3$ m/s, $\Delta T = 8.6$ msec)	19
Fig. 28	Load histories of the ATD lower-tibia axial direction force Fz in the loading condition X065_04 ($\Delta V = 6.5$ m/s, $\Delta T = 4.5$ msec).....	20
Fig. 29	Load histories of the ATD lower-tibia axial direction force Fz in the loading condition X065_08 ($\Delta V = 6.4$ m/s, $\Delta T = 8.6$ msec).....	20
Fig. 30	Load histories of the ATD lower-tibia axial direction force Fz in the loading condition X065_10 ($\Delta V = 6.5$ m/s, $\Delta T = 10.6$ msec)	21
Fig. 31	Relation between the peak load and pulse duration in the ATD lower-tibia axial force Fz.....	22
Fig. 32	Rotation-angle histories of the boot sole against the horizontal line in the experiment.....	23
Fig. 33	Representative ATD lower-leg motion in the experiment, X065_08_03 ($\Delta V = 6.3$ m/s, $\Delta T = 8.6$ msec)	23
Fig. 34	Schematic of the ATD lower-leg loading mechanics for 3 durations of loading.....	25
Fig. 35	Relation between the peak load and pulse duration in the ATD lower- tibia axial force Fz with the peak acceleration of the loading pulse	26

List of Tables

Table 1	FE material models for the floor-mat and floor-plate parts	2
Table 2	Loading conditions for the lower-leg FEA	4
Table 3	Specifications of sensors used in the ATD lower-leg loading test.....	8
Table 4	Loading conditions for the ATD lower-leg loading test	9
Table 5	Summary of experimental results.....	10
Table 6	Summary of experimental results.....	21

Acknowledgments

This report was written by the author in the Engineer Scientist Exchange Program in the US Army Research Laboratory (ARL) from April 2013 to September 2014. I would like to take this opportunity to thank the ARL for giving me the chance to learn and investigate blast-loading issues in the state-of-the-art research environment. Especially, I would like to mention that the Crew Survivability Blast Effects Simulator played an important role in this study to confirm the complex mechanics of the lower-leg loading in the laboratory environment. I also would like to thank the members of the Blast Protection Branch and its specialists for supporting the numerical analysis, experiment, data processing, and various discussions that gave me valuable ideas.

1. Introduction

Lower leg injury is a major injury mode induced by under body blast loading associated with IED (improvised explosive device) attacks against ground fighting vehicles.¹⁻⁴ Blast- mitigating floor mats are regarded as an effective countermeasure for injury prevention,^{5,6} and the methodology for their selection and optimization is in immediate need. However, the loading mechanics in the lower leg in the presence of the floor mat is not fully understood. Thus, we determined a need to clarify the mechanics through the Finite Element Analysis (FEA) by combining the Hybrid III 50th Percentile Anthropomorphic Test Device (ATD) lower leg and the butyl-rubber floor mat.

In this study, we conducted the FEA and experiments on the ATD lower-leg loading in various conditions. Then, we clarified the stress distribution on the boot sole and investigated the correlation between the foot motion and lower-tibia load that is a major criterion for the lower leg injury. Moreover, we focused on the influence of the pulse duration in the ATD lower-tibia force and clarified the loading mechanics from this point of view.

2. Analysis and Experiment Methods

2.1 Finite Element Model

The finite element (FE) model was built on LS-DYNA for the ATD lower-leg loading with the butyl-rubber floor mat, as shown in Fig. 1. In this model, the lower-leg part was composed of the boot and the right leg from the Hybrid III 50th Percentile ATD FE model developed by Livermore Software Technology Corporation (LSTC). The lower-leg part was positioned in the 0–90–0 configuration, and the boot sole was settled on the floor mat to touch the surface. The butyl-rubber floor mat was composed of 2 sheets; the dimensions of each sheet were 8 inches \times 8 inches \times 20 millimeters (mm).

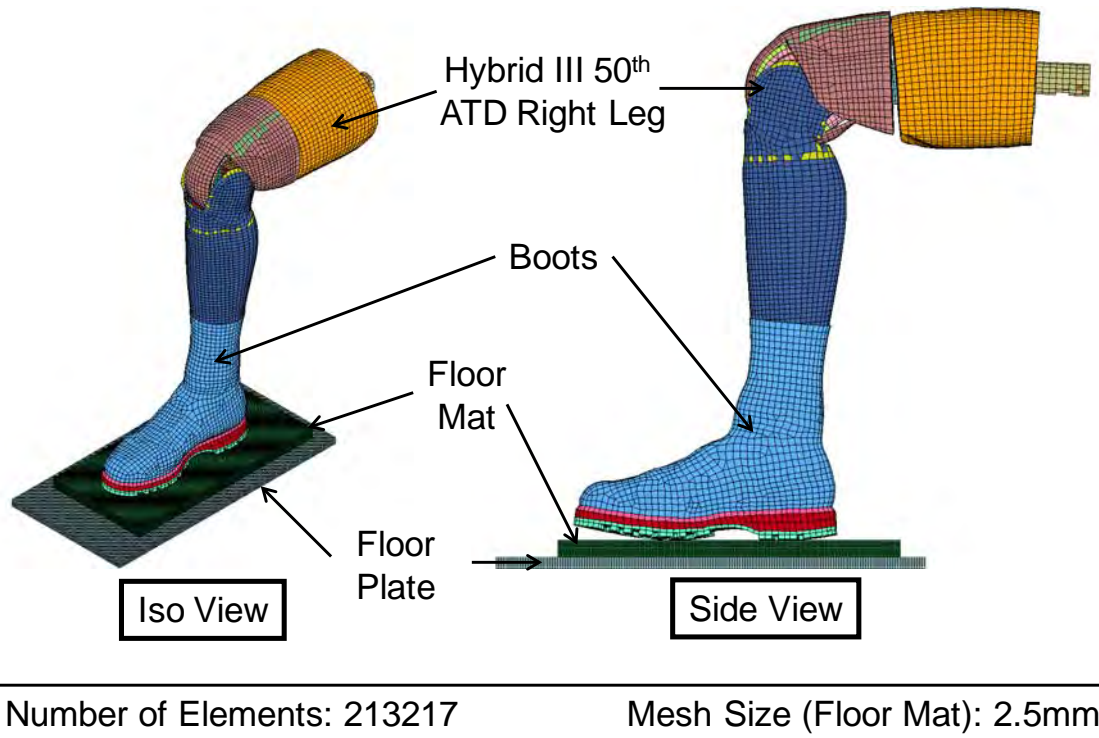


Fig. 1 FE model for the ATD lower-leg loading

The material cards used for the floor mat and floor plate are listed in Table 1. The FE material model for the butyl rubber was the ARL model; a previous report concluded that this model was suitable for the analysis of underbody blast-loading events.⁷ The ARL model showed high accuracy, especially in 4–8-millisecond (msec) pulse loading with 3.0–6.0 meters per second (m/s) velocity change.

Table 1 FE material models for the floor-mat and floor-plate parts

Part	Material	Model Type in LS-DYNA	Model Description /Parameters
Floor Mat	Butyl Rubber	MAT_183_ SIMPLIFIED_RUBBER_ WITH_DAMAGE	Incompressible Rubber Model with Strain-Rate Dependent Loading / Unloading Curves
Floor Plate	Aluminum	MAT_020_ RIGID	RO=2.816e-6 (kg/mm ³) E=70 (GPa) PR=0.30

In this study, we focused on the lower-tibia load and boot-sole load for the clarification of the ATD lower-leg loading mechanics. The lower-tibia loads, F_x, F_y, and F_z, were measured as the section force in the ATD tibia bone as shown in Fig. 2.

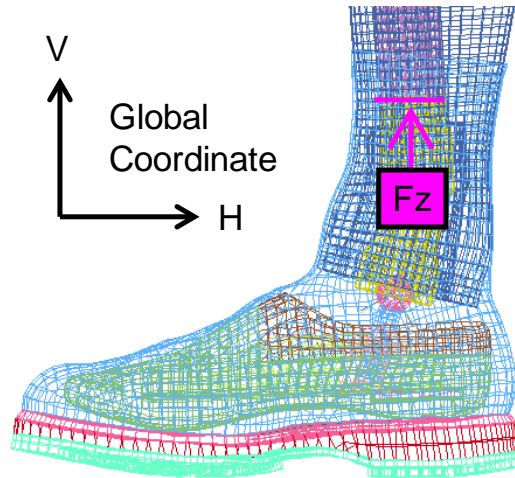


Fig. 2 Definition of the lower-tibia load F_z in the ATD lower-leg FE model

As will be discussed in Section 3, there were distinct high-stress areas in the toe part and heel part on the boot sole. Therefore, we defined the toe part and heel part (Fig. 3) and measured the applied loads respectively. Moreover, an SAE600 filter was applied to each load output in LS-Prepost.

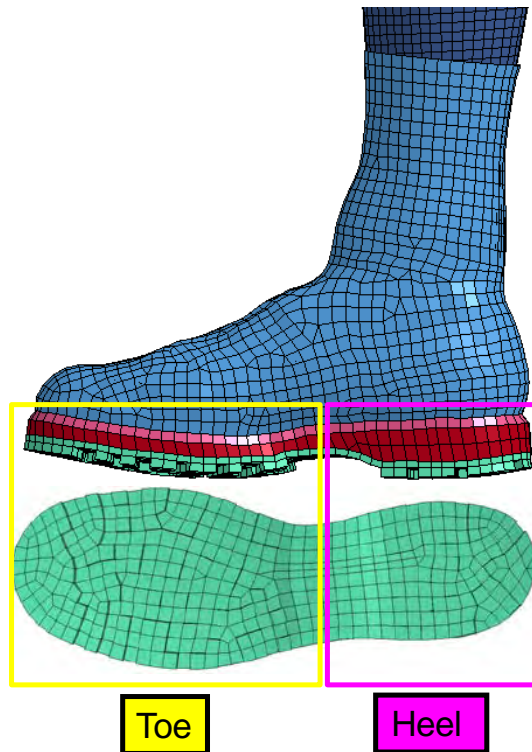


Fig. 3 Definition of the toe part and heel part on the boot sole

2.2 Loading Conditions in the FEA

To clarify the ATD lower-leg loading mechanics, the loading conditions listed in Table 2 were planned for the FEA.

Table 2 Loading conditions for the lower-leg FEA

Velocity Change on the Floor Plate, ΔV (m/s)	Pulse Duration, ΔT (msec)	Condition Code
3.0	2	X030_02
	4	X030_04
	6	X030_06
	8	X030_08
	10	X030_10
6.5	2	X065_02
	4	X065_04
	6	X065_06
	8	X065_08
	10	X065_10
10.0	2	X100_02
	4	X100_04
	6	X100_06
	8	X100_08
	10	X100_10

These loading conditions were applied to the FE model as the velocity histories on the floor plate. The boundary conditions in the FEA are shown in Fig. 4.

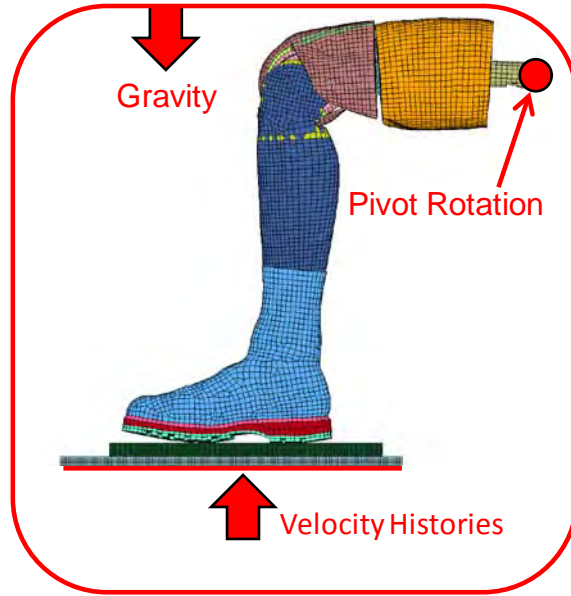


Fig. 4 Schematic of boundary conditions in the FEA

The velocity histories on the floor plate were determined by using the loading conditions and assuming haversine-type acceleration inputs. Moreover, 5-msec initialization phases were considered in the velocity histories for the lower-leg FE model to be settled down on the floor mat. Thus, the velocity history shown in Figs. 5–7 was generated on the floor plate in each loading condition.

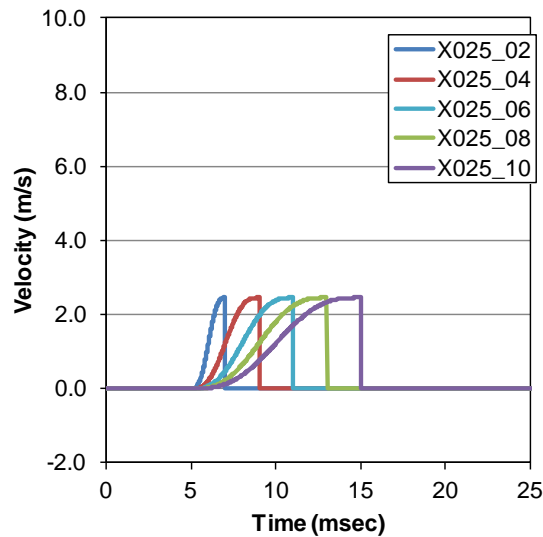


Fig. 5 Velocity histories on the floor plate in FEAs for 3.0-m/s loading

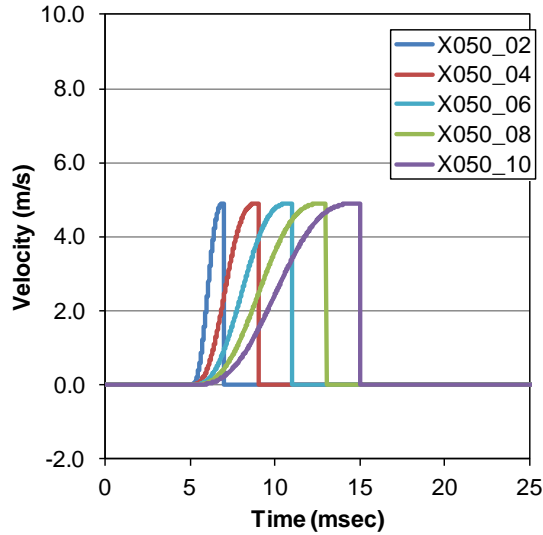


Fig. 6 Velocity histories on the floor plate in FEAs for 6.5-m/s loading

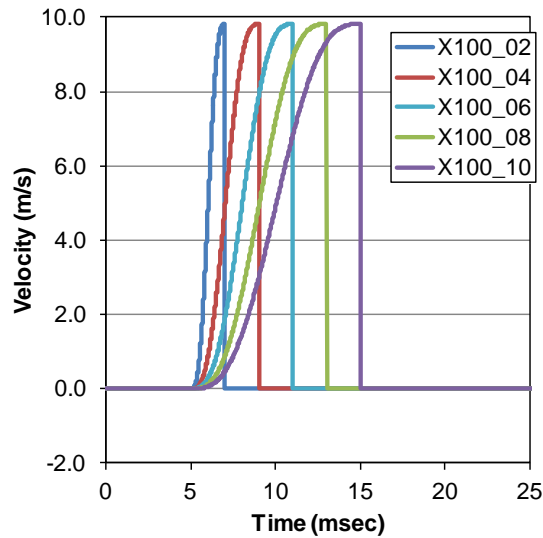


Fig. 7 Velocity histories on the floor plate in FEAs for 10-m/s loading

2.3 Lower-Leg Loading Test

The lower-leg loading test was conducted on the Crew Survivability Blast Effects Simulator (CSBES) at the Adelphi Laboratory Center, ARL. As shown in Fig. 8, the whole body of the Hybrid III 50th Percentile ATD (I-Dummy) was used in this experiment. However, only the local loading function (Floor Motion Simulator) was activated in the CSBES to load the ATD lower leg as the loading in the FEA. The test setup was adjusted in the same way as the FE model: the ATD lower leg with boot was positioned in the 0–90–0 configuration on the floor mat, and the boot sole was settled on the floor mat to touch the surface.

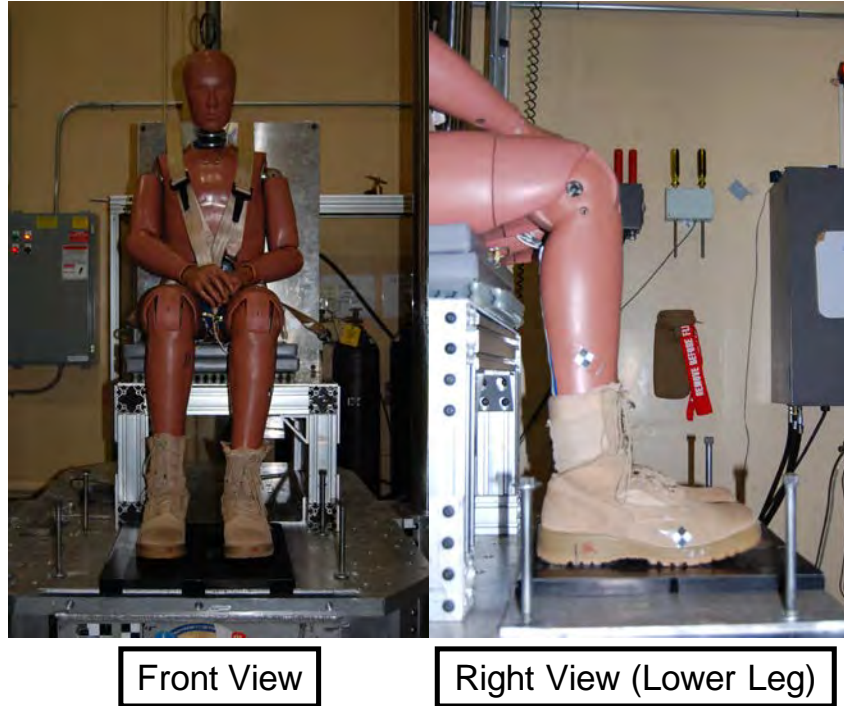


Fig. 8 Test setup for the lower leg loading test with the whole-body ATD and floor mat

The floor mat was composed of 4 sheets of butyl rubber (Fig. 9), and the dimensions of each sheet were 8 inches \times 8 inches \times 20 mm. The sheets at first were replaced by new ones at every shot but later reused after the confirmation of the material's condition. The interval between the usages of a sheet was kept to more than an hour for the material's relaxation.

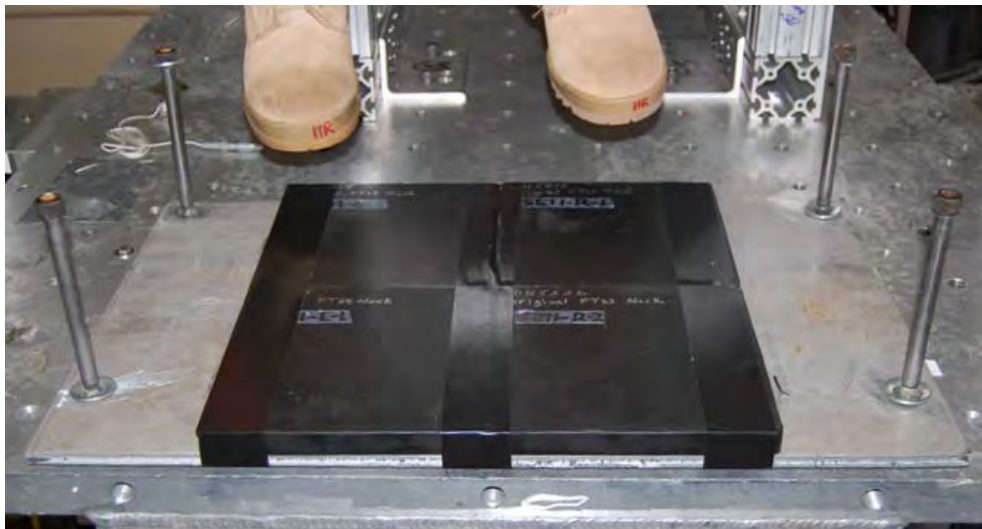


Fig. 9 Sheets of the butyl rubber as the floor mat on the CSBES floor plate

The arrangements of sensors in the test setup are shown in Fig. 10, and the specifications are listed in Table 3. The signals from sensors were recorded in the data-acquisition systems

(Spectral Dynamics’s VXI Model VX2824 and Diversified Technical Systems’ SLICE) at the sampling frequency of 250 kHz. Then, direct-current offset and filters (Table 3) were applied to each signal in postprocessing on the data-analysis software (MathWorks, MATLAB). The test was also recorded by the high-speed imaging camera (Phantom, Miro) for the confirmation of the contact between the boot sole and floor mat.

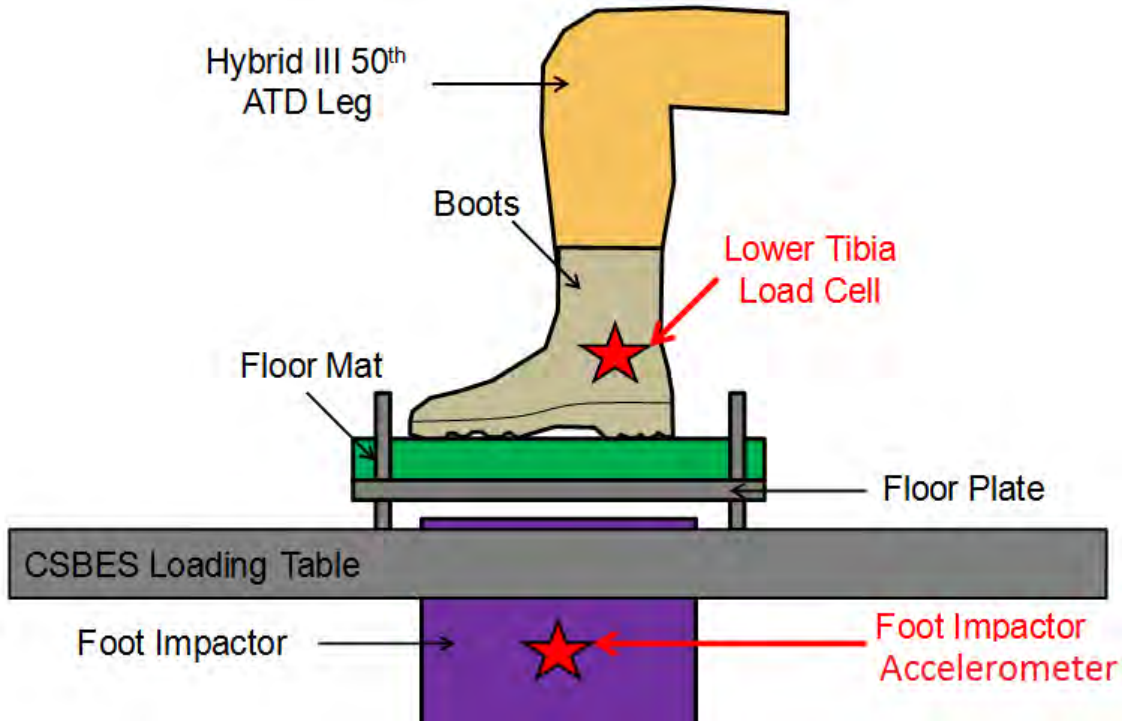


Fig. 10 Arrangements of sensors in the test setup

Table 3 Specifications of sensors used in the ATD lower-leg loading test

Sensor	Position	Type	Range	Filter
Accelerometer	Foot Impactor (Left)	Endevco 7270A-20KM6	20000G	CFC1000
Accelerometer	Foot Impactor (Right)	Endevco 7270A-60KM6	60000G	CFC1000
Load cell	Lower Tibia (Left & Right)	Denton 3644JDI450	2500lbf	CFC600

As will be discussed, the FEA results indicated there was a relation between the pulse duration and peak load in the ATD lower tibia. Therefore, the loading conditions listed in Table 4 were planned to confirm the relation through the experiment.

Table 4 Loading conditions for the ATD lower-leg loading test

Velocity Change on the Floor Plate, ΔV (m/s)	Pulse Duration, ΔT (msec)	Condition Code
6.5	4	X065_04
	8	X065_08
	10	X065_10

3. Results and Discussion

3.1 FEA Results

Representative load histories of the ATD lower tibia in the FEA are shown in Fig. 11, and FEA results are summarized in Table 5. As compared with the lower-tibia axial force F_z , the perpendicular forces F_x and F_y are much smaller; the ATD lower tibia is probably loaded vertically through the boot heel. Therefore, we mainly focus on F_z in the following discussion.

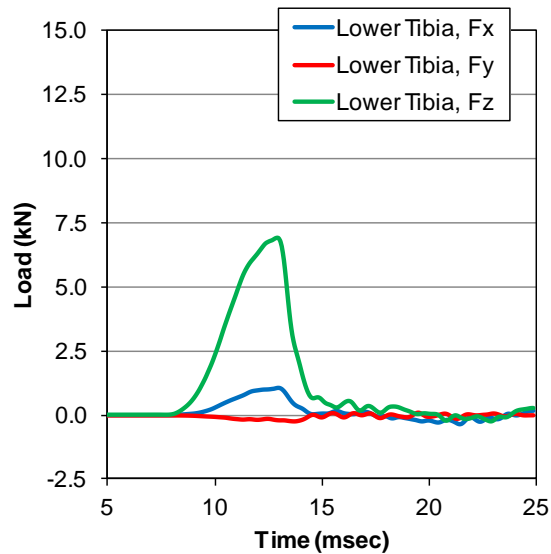


Fig. 11 Representative load histories of the ATD lower tibia in the FEA, X065_08 ($\Delta V = 6.5$ m/s, $\Delta T = 8$ msec)

Table 5 Summary of experimental results

Loading Condition	Velocity Change, ΔV (m/s)	Pulse Duration, ΔT (msec)	Peak Lower Tibia Load, F_z (kN)	Applied Impulse (Nsec)
X030_02	3.0	2	0.7	4.4
X030_04		4	1.6	5.6
X030_06		6	2.2	7.6
X030_08		8	2.6	9.1
X030_10		10	2.6	10.9
X065_02	6.5	2	2.9	10.0
X065_04		4	2.6	14.2
X065_06		6	6.8	19.4
X065_08		8	6.9	23.9
X065_10		10	6.6	26.0
X100_02	9.8	2	5.6	16.4
X100_04		4	10.3	24.2
X100_06		6	12.4	32.7
X100_08		8	12.6	41.3
X100_10		10	11.3	49.2

A typical ATD foot motion in the FEA is shown in Fig. 12. In the initial loading phase, the floor plate and floor mat translate upward as one, and the boot sole sinks into the floor mat. In the following phase, the foot rotates slightly around the ankle joint, and the boot toe possibly loses contact with the floor mat.

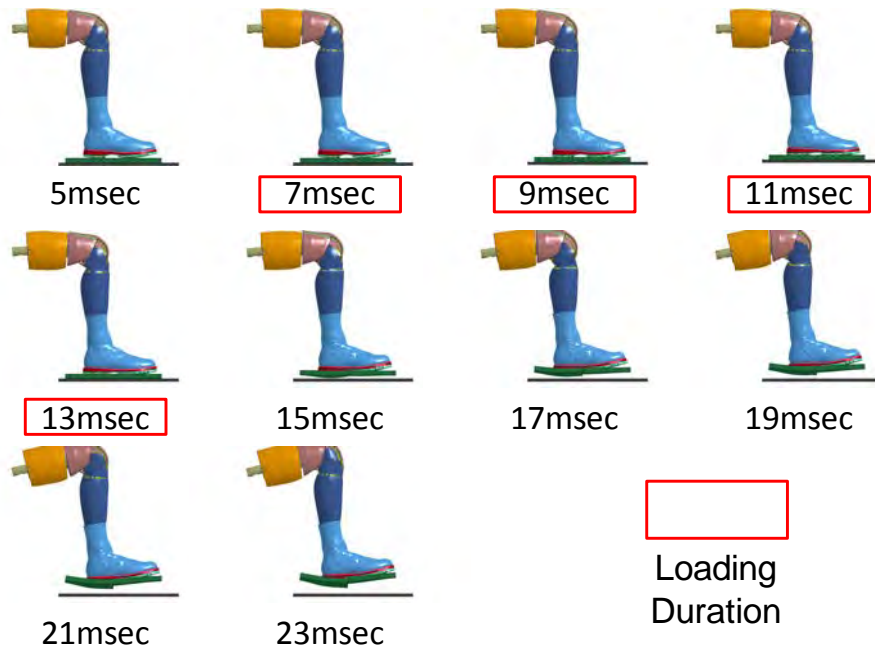


Fig. 12 Representative ATD lower-leg motion in the FEA, X065_08 ($\Delta V = 6.5$ m/s, $\Delta T = 8$ msec)

As shown in Figs. 13–15, representative pressure distributions on the footprint also indicate this motion. The boot toe does not always touch the floor mat during the loading, although the boot heel is pressed onto the floor mat during the whole period of the loading.

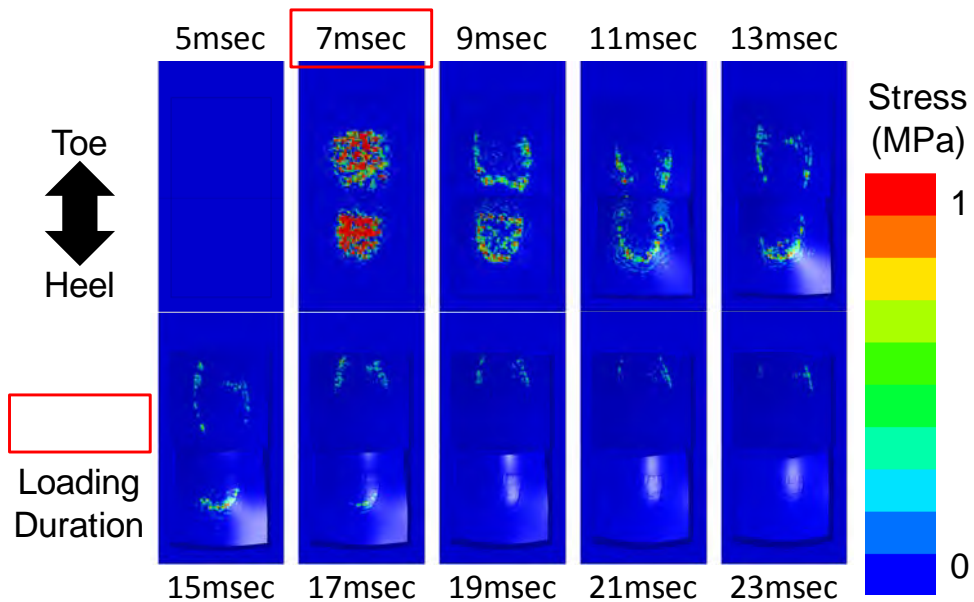


Fig. 13 Pressure distribution under the boot sole in the FEA result, X065_02 ($\Delta V = 6.5$ m/s, $\Delta T = 2$ msec)

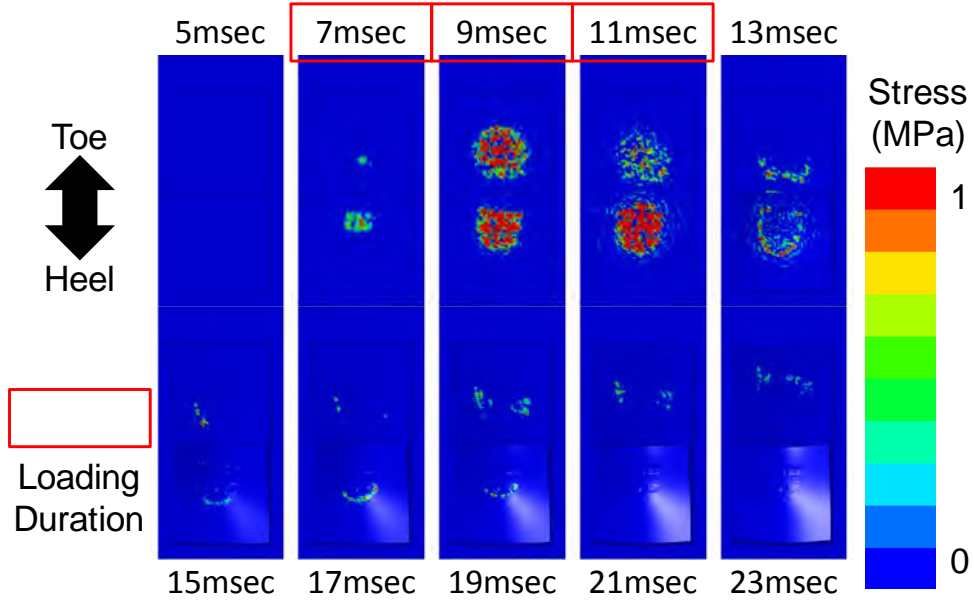


Fig. 14 Pressure distribution under the boot sole in the FEA result, X065_06 ($\Delta V = 6.5$ m/s, $\Delta T = 6$ msec)

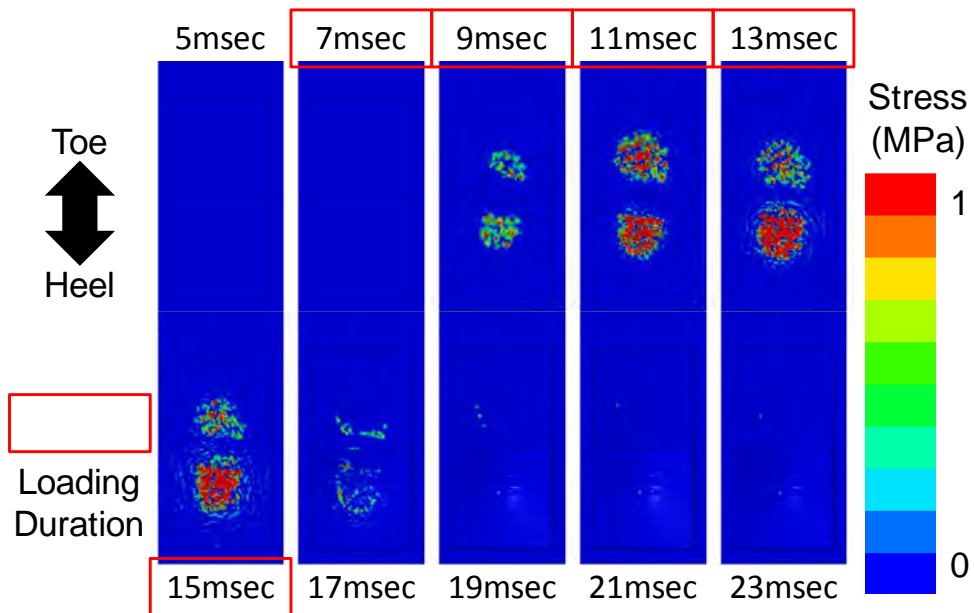


Fig. 15 Pressure distribution under the boot sole in the FEA result, X065_10 ($\Delta V = 6.5$ m/s, $\Delta T = 10$ msec)

Moreover, the load histories on the ATD lower tibia, boot toe, boot heel, and whole boot are shown in Figs. 16–18 for representative loading conditions. Thus, the pulse duration of the loading probably affects the ATD lower-tibia load. From this point of view, we will discuss the ATD lower-leg loading mechanics later in this report.

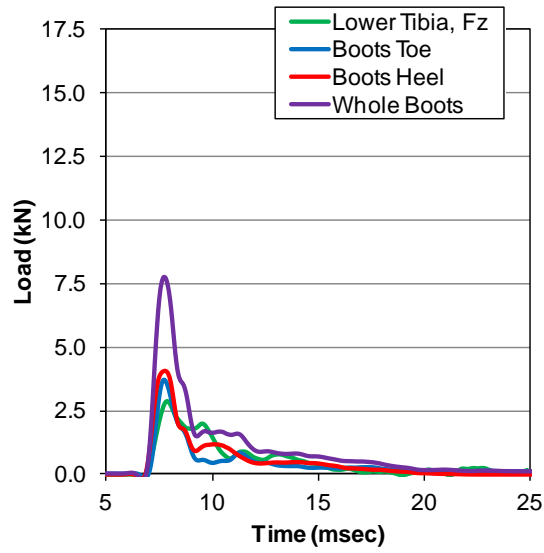


Fig. 16 Example of load histories of the ATD lower leg in the FEA, X065_02 ($\Delta V = 6.5$ m/s, $\Delta T = 2$ msec)

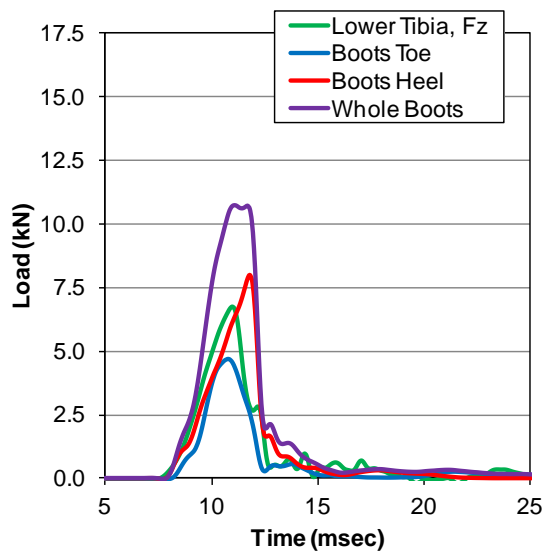


Fig. 17 Example of load histories of the ATD lower leg in the FEA, X065_06 ($\Delta V = 6.5$ m/s, $\Delta T = 6$ msec)

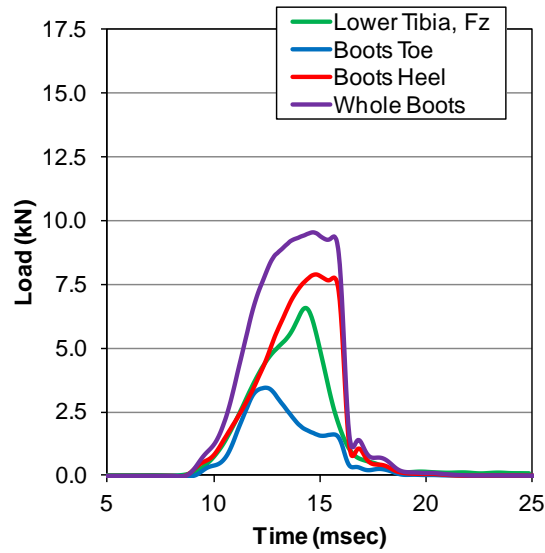


Fig. 18 Example of load histories of the ATD lower leg in the FEA, X065_10 ($\Delta V = 6.5$ m/s, $\Delta T = 10$ msec)

The relation between the peak load and pulse duration on each interface are shown in Figs. 19 and 20 for a representative velocity change of 6.5 m/s.

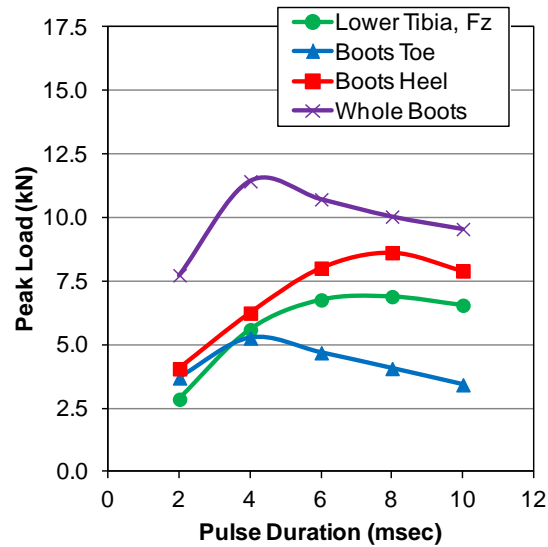


Fig. 19 Example of the relation between the peak load and pulse duration on various interfaces in the ATD lower leg, X065 series ($\Delta V = 6.5$ m/s)

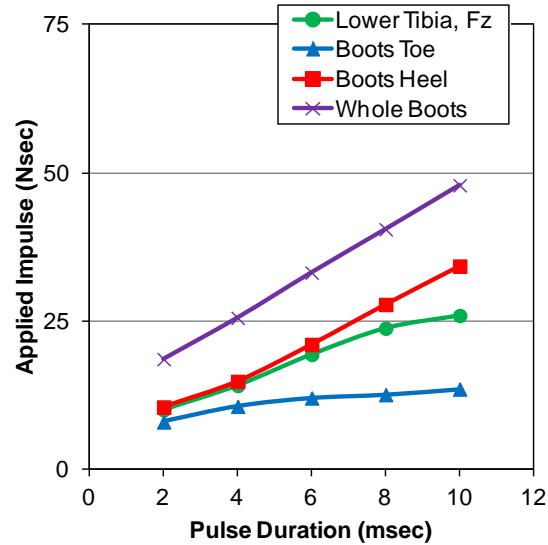


Fig. 20 Example of the relation between the applied impulse and pulse duration on various interfaces in the ATD lower leg, X065 series ($\Delta V = 6.5$ m/s)

Moreover, the peak loads and applied impulses in the ATD lower tibia are summarized for various loading conditions in Figs. 21 and 22. Then, the peak loads of the ATD lower tibia and boot heel are increasing between 2 and 8 msec as the pulse duration increases, whereas those of boot toe are decreasing except for 2 msec. Note also that the applied impulse is clearly increasing on every interface, although the increase on the boot toe is small.

The ATD lower-tibia loads in short-duration loadings are expected to be higher than those of long-duration loadings with the same ΔV because the acceleration in the loading pulse is higher. However, the FEA results indicate the opposite tendency as discussed above. This is probably caused by the change in the contact status on the boot sole because the impulse is increasing (as shown in Fig. 20).

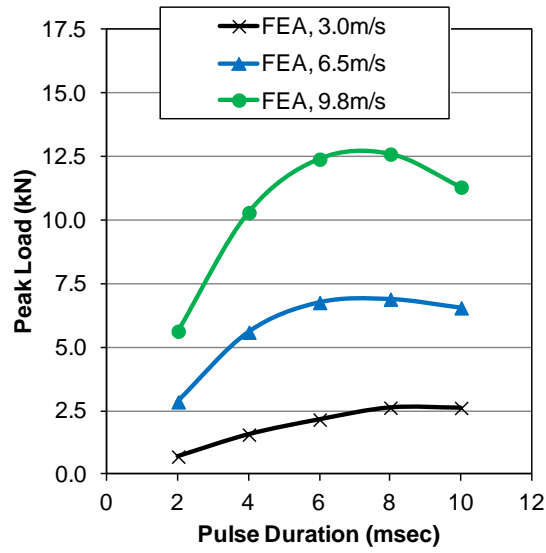


Fig. 21 Relation between the peak load and pulse duration in the ATD lower-tibia axial force F_z from FEA results

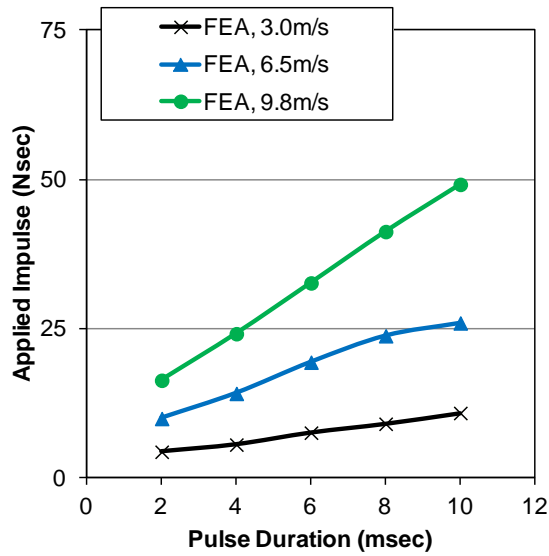


Fig. 22 Relation between the applied impulse and pulse duration in the ATD lower-tibia axial force F_z from FEA results

The interactions among the ATD foot, boot, and floor mat are shown in Figs. 23–25 for representative loading conditions.

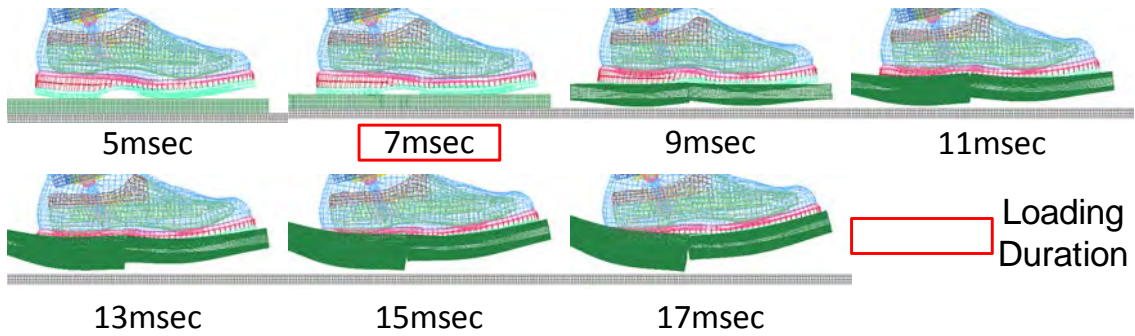


Fig. 23 Interaction among the ATD foot, boot, and floor mat, X065_02 ($\Delta V = 6.5 \text{ m/s}$, $\Delta T = 2 \text{ msec}$)

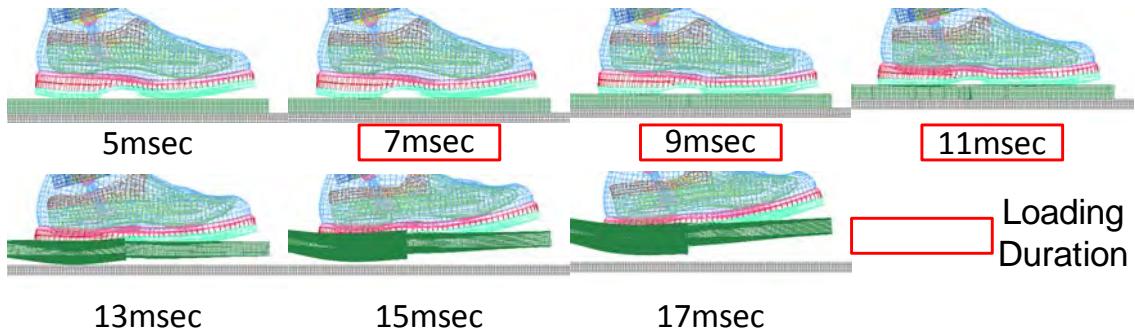


Fig. 24 Interaction among the ATD foot, boot, and floor mat, X065_06 ($\Delta V = 6.5 \text{ m/s}$, $\Delta T = 6 \text{ msec}$)

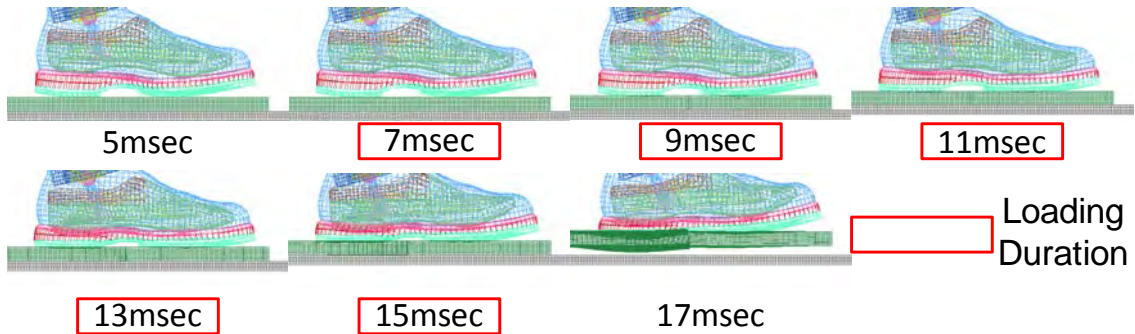


Fig. 25 Interaction among the ATD foot, boot, and floor mat, X065_10 ($\Delta V = 6.5 \text{ m/s}$, $\Delta T = 10 \text{ msec}$)

Moreover, the rotation-angle histories of the boot sole are shown in Fig. 26 for a representative ΔV ; the validity of the ATD lower-leg FE model is not quantitative but qualitative in the rotational movement around the ankle joint. Considering these boot-sole contact data, the following phases now are assumed for the ATD lower-leg loading:

- 1) In the initial phase of loading, the boot toe and heel are loaded almost uniformly. At this point, the load histories on these 2 interfaces are similar.
- 2) In this phase the boot sole and floor mat start to deform, which causes the arch in the boot sole and the foot to fit the floor mat and the boot insole, respectively. These deformations

increase the contact among the floor mat, boot sole, boot insole, and foot, and enhance transmissibility of the load.

- 3) In the following phase of loading, the foot starts to rotate around the ankle joint. Then, the boot toe loses contact with the floor mat, and the load on the boot toe decreases. The opposite occurs with the boot heel, whose load increases because of its close contact with the floor mat.

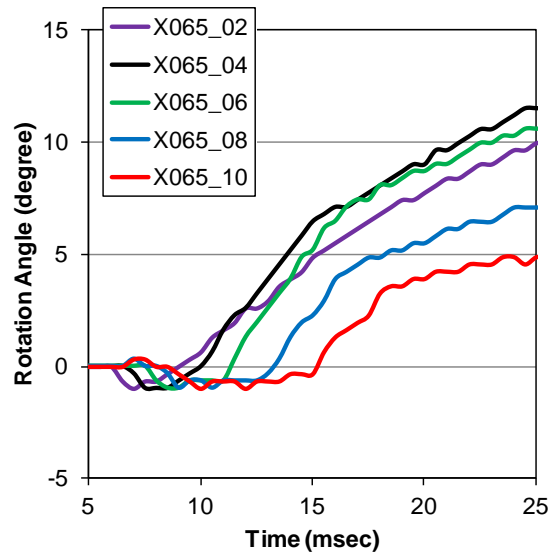


Fig. 26 Rotation-angle histories of the boot sole against the horizontal line in the FEA, X065 series ($\Delta V = 6.5$ m/s)

In short-duration loading (2 and 4 msec), Phases 1 and 2 occur during the loading as shown in Figs. 16, 23, and 26. However, the deformation in Phase 2 is not as large as that in long-duration loading, and the boot sole is not sufficiently compressed during the loading. Moreover, Phase 3 starts after the completion of the loading, and the ATD foot motion does not affect the load profile. Therefore, the load profiles of the boot toe and heel are similar (as shown in Fig. 16), and the peak load is much smaller than that of long-duration loading. By contrast, in long-duration loading (6–10 msec), Phase 3 starts during the loading at the same time as Phases 1 and 2 (as seen in Figs. 17, 25, and 26). Therefore, the boot sole and floor mat contact each other more closely on the boot heel. Together with the deformations in the boot sole and floor mat, this is probably the major cause of the increase in the boot-heel load. Then, as shown in Fig. 17 and 18, the load profiles of the boot toe and heel are different on the latter part of the loading. However, the peak load is slightly decreasing in 10-msec-pulse loading. This is probably due to the decrease of the peak acceleration in the loading pulse.

Considering that the ATD lower tibia is loaded vertically, the load profiles of the boot heel are reflected in those of the ATD lower tibia, including its pulse-duration dependency. Therefore, the peak load in the ATD lower tibia probably shows the curve with an inflection point as shown in

Fig. 19. This hypothesis on the ATD lower-leg loading mechanics will be confirmed in the following discussion of the experiment.

3.2 Experimental Results

Representative loading histories of the ATD lower tibia are shown in Fig. 27. In the ATD lower tibia, the perpendicular forces F_x and F_y are much smaller than the axial force F_z as in the FEA results.

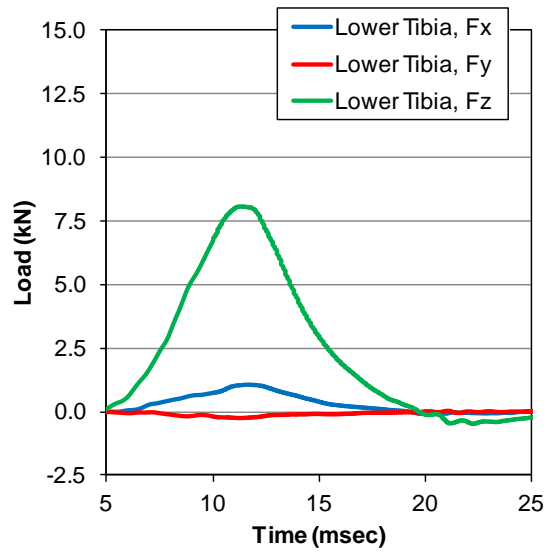


Fig. 27 Representative load histories of the ATD lower tibia in the experiment, X065_06_03 Right Leg ($\Delta V = 6.3$ m/s, $\Delta T = 8.6$ msec)

The load histories are shown in Figs. 28–30 for each loading condition and experimental results are summarized in Table 6. The deviation of the test results in each loading condition is less than 10%—less than 5% in the peak load—which is believed to be small enough for the detailed comparison that follows.

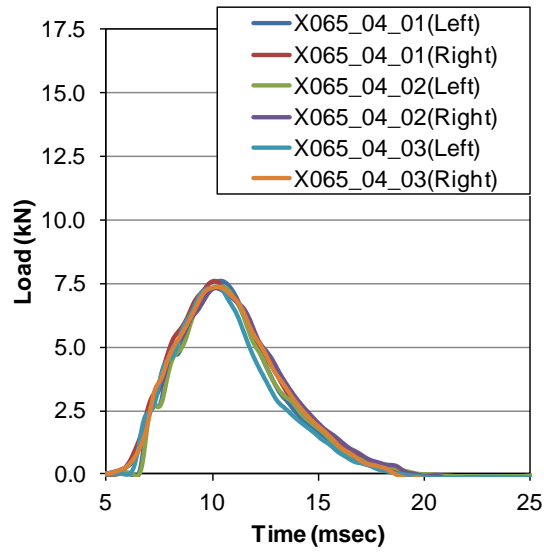


Fig. 28 Load histories of the ATD lower-tibia axial direction force F_z in the loading condition X065_04 ($\Delta V = 6.5$ m/s, $\Delta T = 4.5$ msec)

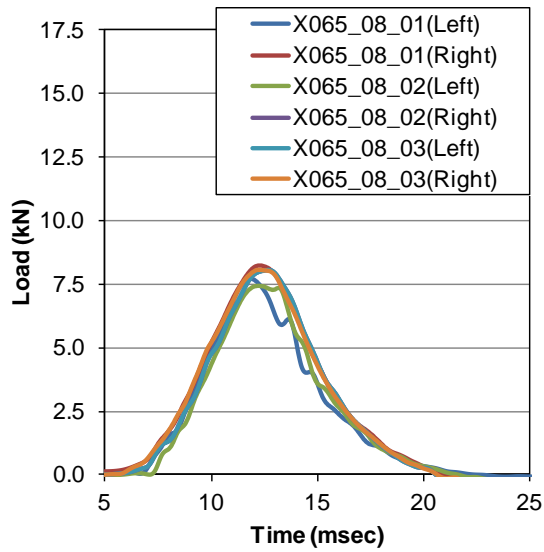


Fig. 29 Load histories of the ATD lower-tibia axial direction force F_z in the loading condition X065_08 ($\Delta V = 6.4$ m/s, $\Delta T = 8.6$ msec)

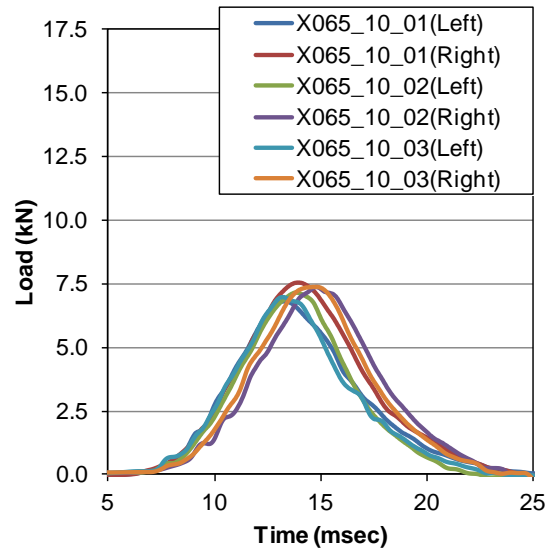


Fig. 30 Load histories of the ATD lower-tibia axial direction force F_z in the loading condition X065_10 ($\Delta V = 6.5$ m/s, $\Delta T = 10.6$ msec)

Table 6 Summary of experimental results

Shot Code	Foot Impactor Velocity Change, ΔV Left / Right (m/s)	Pulse Duration, ΔT Left / Right (msec)	Peak Lower Tibia Load Left / Right (kN)	Applied Impulse Left / Right (Nsec)
X065_04_01	6.4 / 6.7	4.5 / 4.6	7.6 / 7.6	41.4 / 45.8
X065_04_02	6.4 / 6.4	4.5 / 4.5	7.4 / 7.3	41.2 / 45.7
X065_04_03	6.3 / 6.6	4.5 / 4.7	7.4 / 7.4	39.8 / 44.5
Avg. / SD	6.5 / 2%	4.5 / 2%	7.5 / 2%	43.1 / 6%
X065_08_01	6.6 / 6.4	8.5 / 8.8	7.7 / 8.2	45.6 / 53.2
X065_08_02	6.6 / 6.1	8.7 / 8.8	7.4 / 8.1	45.0 / 50.0
X065_08_03	6.5 / 6.1	8.7 / 8.4	8.1 / 8.0	49.0 / 51.8
Avg. / SD	6.4 / 3%	8.6 / 2%	7.9 / 4%	49.1 / 7%
X065_10_01	6.5 / 6.6	10.1 / 10.6	6.8 / 7.6	47.2 / 53.9
X065_10_02	6.2 / 6.6	10.8 / 10.9	7.2 / 7.4	45.1 / 51.8
X065_10_03	6.3 / 6.9	10.8 / 10.5	7.0 / 7.4	45.2 / 51.5
Avg. / SD	6.5 / 4%	10.6 / 3%	7.2 / 4%	49.1 / 8%

As shown in Fig. 31, the differences between the FEA results and experimental results are at most 20% in the peak load of the ATD lower tibia. However, as shown in Figs. 11 and 27, the

duration of the response pulse in the experiment is significantly longer than that in the FEA on the same loading condition. In the CSBES loading test, the loading profile in the floor plate is determined by the interaction between the foot impactor and upper mass (such as ATD leg and boot and the floor plate). Therefore, the velocity histories on the floor plate are not the same as those of the FEAs in Fig. 5–7, although the acceleration histories are the same between the floor plate in FEA and foot impactor in the experiment. Thus, the actual duration of the loading pulse on the boot sole is longer than that in the FEA. This probably leads to the longer-duration response in the experiment and should be considered in the following discussion.

As to the lower-leg loading, the tendency is basically the same as that assumed on the FEA results; the peak load in the ATD lower tibia shows a curve with an inflection point as shown in Fig. 31. However, the tendency is not as clear as that of the FEA results, especially in the short-duration loading (4 msec).

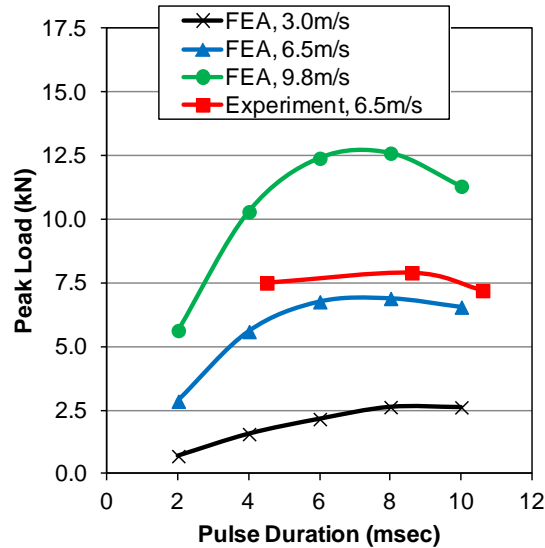


Fig. 31 Relation between the peak load and pulse duration in the ATD lower-tibia axial force F_z

A typical ATD foot motion in the experiment is shown in Fig. 32, and the rotation-angle histories of the boot sole are shown in Fig. 33. These show that the differences of the rising time and maximum angle of the foot rotation are smaller than those of the FEA results; this is probably because the rotational restriction around the ATD ankle joint was not perfectly controlled in the experiment. Therefore, together with the longer-duration response, this leads to the smaller difference of the peak load in the experiment.

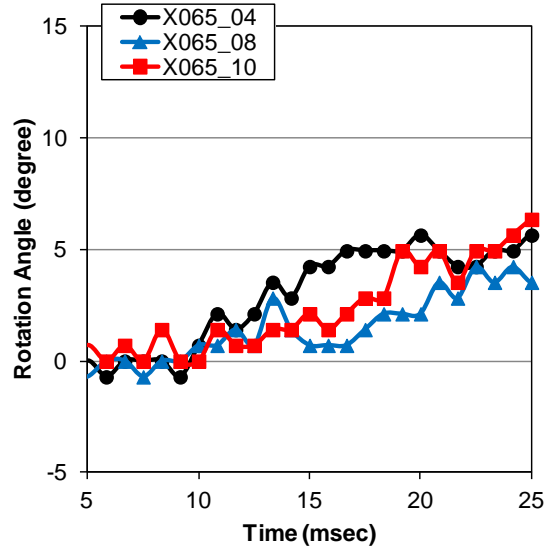


Fig. 32 Rotation-angle histories of the boot sole against the horizontal line in the experiment

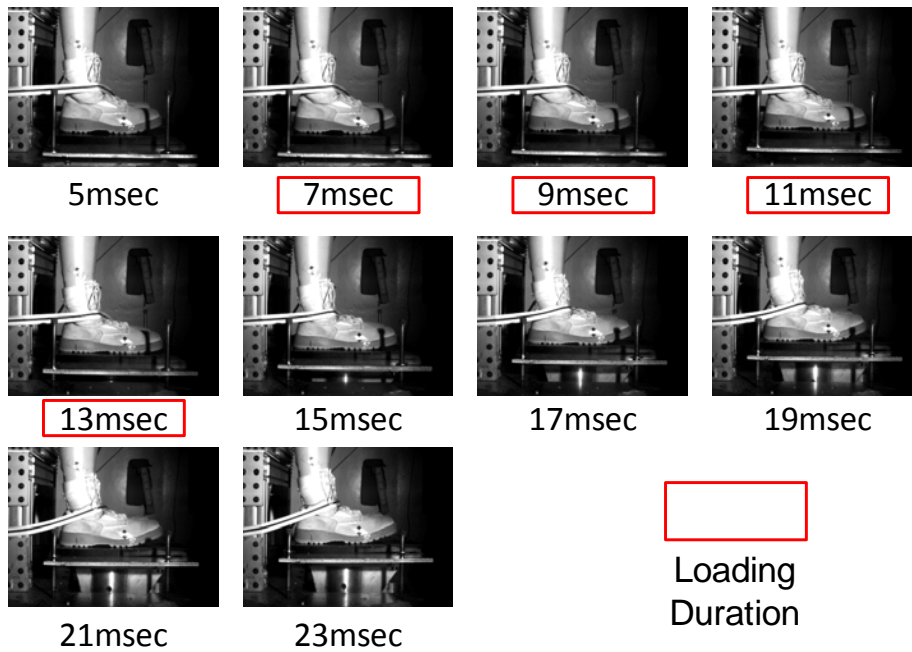


Fig. 33 Representative ATD lower-leg motion in the experiment, X065_08_03 ($\Delta V = 6.3$ m/s, $\Delta T = 8.6$ msec)

3.3 ATD Lower-Leg Loading Mechanics

The ATD lower-leg loading mechanics suggested by the FEA results have been confirmed qualitatively through the experimental results. According to the discussion in Sections 3.1 and 3.2, the pulse duration of the loading is categorized into 3 types, and the loading mechanics are restructured as follows (see also the schematic in Fig. 34):

- 1) In short-duration loading (2 msec), the boot sole deforms only slightly. Moreover, the foot rotation starts after the completion of the loading. Therefore, the loading pulse is not fully transmitted to the ATD lower tibia, and the peak load is smaller than that of longer-duration loading.
- 2) In middle-duration loading (4, 6, and 8 msec), both boot-sole deformation and foot rotation occur during the loading, and the loading pulse is fully transmitted to the ATD lower tibia. Therefore, as shown in Fig. 35, the peak load increases in spite of the decrease in the peak acceleration in the loading pulse.
- 3) In long-duration loading (10 msec), the loading mechanics are almost the same as that of the middle-duration loading, and the boot sole and floor mat closely contact. However, the decrease in the peak acceleration in the loading pulse probably leads to the decrease in the peak load under the close contact between the boot sole and floor mat.

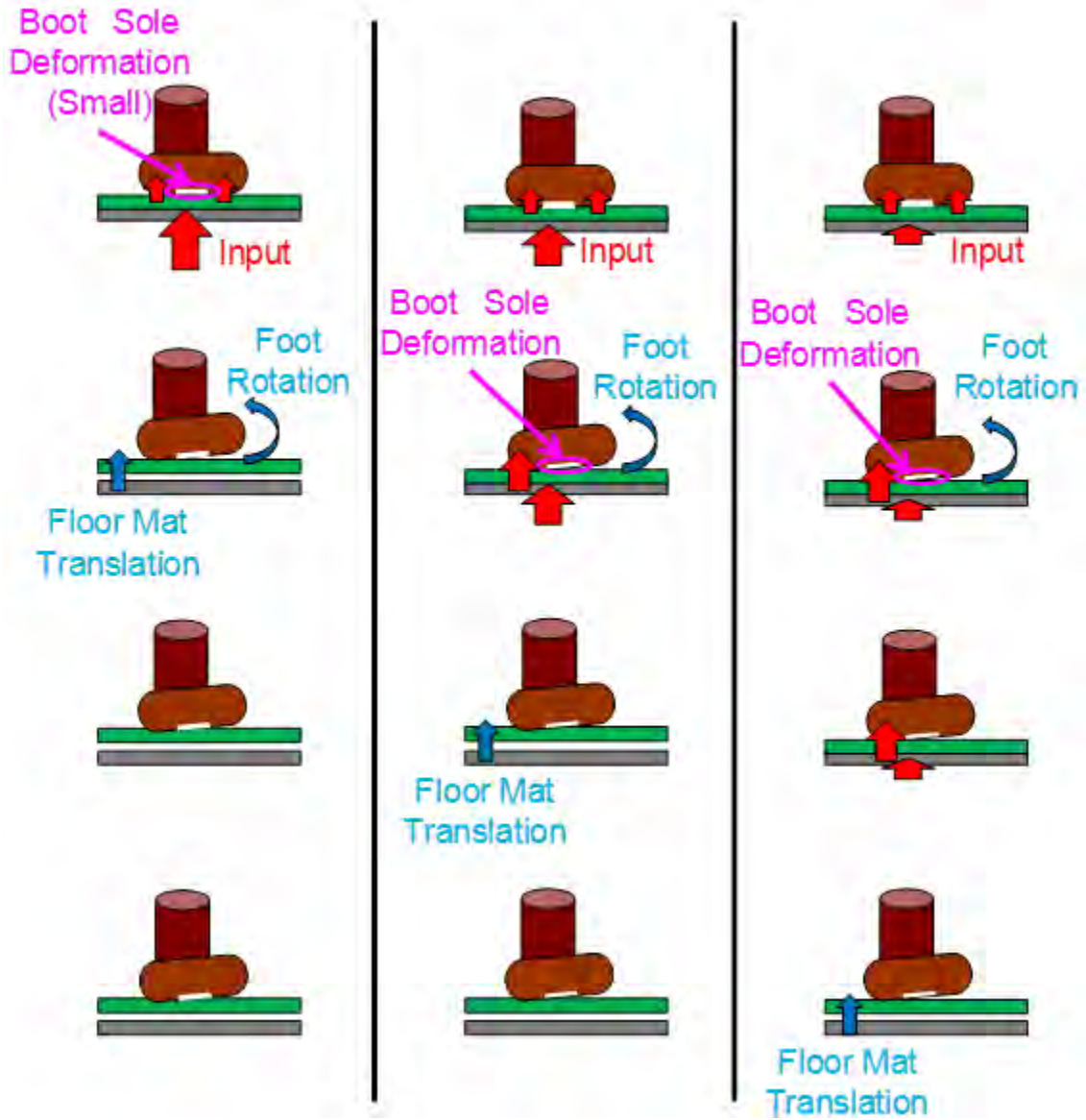


Fig. 34 Schematic of the ATD lower-leg loading mechanics for 3 durations of loading

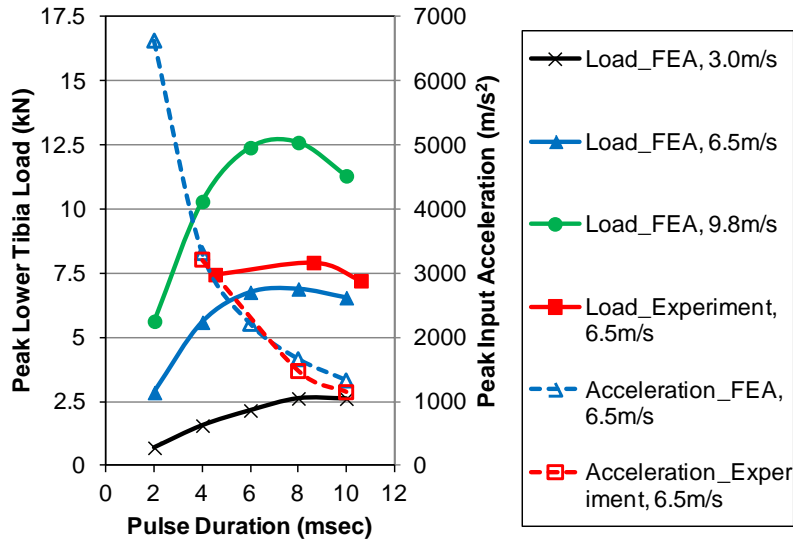


Fig. 35 Relation between the peak load and pulse duration in the ATD lower-tibia axial force F_z with the peak acceleration of the loading pulse

4. Conclusions

In this study, we conducted the FEA of the ATD lower-leg loading to clarify the loading mechanics with the existence of the butyl-rubber floor mat. According to the FEA results, we proposed a hypothesis that the peak load in the ATD lower tibia had a dependency on the pulse duration of loading. We qualitatively confirmed this hypothesis through the ATD lower-leg loading test. Further, the ATD lower-leg loading mechanics have been clarified with these 3 conclusions:

- 1) The ATD lower tibia is loaded almost vertically through the boot heel.
- 2) The peak load in the ATD lower tibia is dependent on the pulse duration of loading; the longer-duration loading under the same ΔV leads to the higher peak load in the ATD lower tibia, whereas there is an exemption due to the low peak acceleration in the loading pulse.
- 3) The deformation of the boot sole and rotation of the foot have an effect on the dependency; in long-duration loading, the boot sole and floor mat contact more closely, and this enhances the transmissibility of the load.

Conclusion 2 is significant. Generally, shock-mitigating countermeasures including floor mats tend to decrease the peak value (acceleration, load) of loading. Moreover, that lengthens the pulse duration of loading under the law of conservation of momentum. However, according to Conclusion 2, this may lead to higher peak load in the ATD lower tibia. Therefore, several

loading tests with different pulse durations are recommended in the evaluation of countermeasures so as to not overestimate the efficiency of the long-duration loading.

5. References

1. Dougherty AL, Mohrle CR, Galarneau MR, Woodruff SI, Dye JL, Quinn KH. Battlefield extremity injuries in Operation Iraqi Freedom. *Injury*. 2009;40(7):772–777.
2. Belmont PJ, Schoenfeld AJ, Goodman G. Epidemiology of combat wounds in Operation Iraqi Freedom and Operation Enduring Freedom: orthopaedic burden of disease. *J Surg Orthop Adv*. 2010;19(1):2–7.
3. Eskridge SL, Macera CA, Galarneau MR, Holbrook TL, Woodruff SI, MacGregor AJ, Morton DJ, Shaffer RA. Injuries from combat explosions in Iraq: injury type, location, and severity. *Injury*. 2012;43(10):1678–1682.
4. Test methodology for protection of vehicle occupants against anti-vehicular landmine effects. NATO; 2007. Report No.: TR-HFM-090.
5. Golan G, Asaf Z, Ran E, Aizik F. Occupant legs survivability: an assessment through the utilization of field blast test methodology. Paper presented at: MABS22. Proceedings of the 22nd International Symposium on Military Aspects of Blast and Shock; 2012 Nov 4–9; Bourges, France.
6. Dong L, Zhu F, Jin X, Suresh M, Jiang B, Sevagan G, Cai Y, Li G, Yang KH. Blast effect on the lower extremities and its mitigation: a computational study. *J Mech Behav Biomed Mater*. 2013;28:111–124.
7. Sakamoto M. Experimental validation of the butyl-rubber finite element (FE) material model for the blast-mitigating floor mat. Adelphi (MD); Army Research Laboratory (US). 2015 Aug. Report No.: ARL-SR-0329.

6. List of Symbols, Abbreviations, and Acronyms

ARL	US Army Research Laboratory
ATD	anthropomorphic test device
CSBES	Crew Survivability Blast Effects Simulator
FE	Finite Element
FEA	Finite Element Analysis
IED	improvised explosive device
kN	kilonewton
LSTC	Livermore Software Technology Corporation
mm	millimeter
msec	millisecond
m/s	meters per second

1 DEFENSE TECH INFO CTR
(PDF) ATTN DTIC OCA

2 US ARMY RSRCH LABORATORY
(PDF) ATTN IMAL HRA MAIL & RECORDS MGMT
ATTN RDRL CIO LL TECHL LIB

1 US ARMY RSRCH LAB
(PDF) ATTN RDRL WMP F R KARGUS